

# Research on Real-time Energy Management Strategy of Dual Motor Coupled PHEV Based on Model Predictive Control

Chao Ma, Yue Shang, Shiwei Jin, Kun Yang, Zhihao Li

**Abstract**—In this paper, model predictive control (MPC) based energy management strategy is developed for dual motor coupled plug-in hybrid vehicle (PHEV) configuration. Firstly, the dynamic characteristics and working mode of dual motor coupled PHEV configuration are analyzed. Secondly, the rule-based strategy and dynamic programming (DP) strategy are developed and selected as the benchmark. Thirdly, vehicle speed prediction accuracy of three different prediction models for various time domain lengths is investigated considering the possibility of real-time applications. Thus, RBF neural network prediction model is applied in the following MPC strategy. Finally, the MPC strategy is developed through the rolling optimization and local optimization of DP strategy, which achieves the optimal torque distribution between engine and motors. Comparative analysis for rule-based, DP and MPC strategies are performed. It is seen that the MPC strategy can obtain similar fuel consumption with DP strategy, while the MPC strategy has certain real-time application potential with only 0.269s per single step calculation time. Compared with the rule-based strategy, the MPC achieves obvious fuel consumption and total cost improvement by 14.5% and 12.6% respectively. Therefore, MPC strategy can effectively improve the fuel economy and has certain real time application potential.

**Index Terms**—Plug in hybrid electric vehicle; Dual motor coupled; Dynamic programming; Model predictive control; Energy management strategy.

## I. INTRODUCTION

As a compromise for new energy vehicles, PHEV has longer driving range and higher fuel economy compared with pure electric vehicles and traditional fuel vehicles [1, 2]. In order to further improve the fuel economy of PHEV, vehicle configuration and energy management strategy have

been studied [3].

In the aspect of vehicle configuration, the operating modes of dynamic coupling configuration of PHEV are investigated to realize the fuel economy improvement [4]. The three-planet coupling configuration [5, 6] has obvious advantages in the transmission system while the improvement of fuel efficiency is inconspicuous. The planetary gear mechanism and clutch power separation system combined configuration [7] can achieve better economy and power performance than the traditional vehicles. Through the coupling of planetary gear mechanism, the PHEV can effectively reduce the total cost [8]. Therefore, the planetary gear coupling mechanism can greatly improve the driving efficiency of PHEV.

Many scholars have carried out studies on energy management strategy (EMS). The EMS can be generally divided into rule-based energy management strategies and optimization-based energy management strategies [9, 10]. In the aspect of rule-based energy management strategies, Liu & Peng have proposed a rule-based strategy about the hybrid configuration of double planetary gears to solve the mode switch of multi-power source [11]. Moreover, the genetic algorithm can optimize the control strategy, which improves the system efficiency [12]. Besides, the intelligent logic rule-based strategy [13] optimizes engine operation range and improves the adaptability to unknown driving conditions. The rule-based energy management strategy has easy implementation and good real-time performance while the adaptability is poor in general.

In the aspect of reducing the fuel and electric consumption of PHEV, Wang & Jiao have proposed Pontryagin's minimum principle and particle swarm optimization strategies to reduce the battery recession of PHEV [14]. The dynamic programming is applied to estimate the optimal-benchmark solution for truck model. Then fuel economy under different control strategies are assessed [15]. Nowadays, the local linear approximation [16] and the convex optimization [17] algorithms can significantly reduce the calculation time of DP algorithm. Particularly, Meo has proved that the nonlinear convex optimization can considerably improve the economic performance of hybrid electric vehicles [18]. The optimization-based algorithms can be applied to the external power grid on PHEV and provide a new idea for energy management strategy [19]. Vajedi & Silva have proposed the equivalent minimum fuel consumption strategy, which can obtain the optimization solution by converting fuel and electricity consumption into an objective function [20, 21].

Manuscript received May 19, 2022; revised Nov 16, 2022.

This work was supported by the National Natural Science Foundation of China (Grant No. 51605265) and the Key Research and Development Program of Shandong Province of China (Grant No. 2019GGX104069).

Chao Ma is an associate professor of College of Transportation and Vehicle Engineering, Shandong University of Technology, Zibo, Shandong, China (e-mail: mc@sdut.edu.cn).

Yue Shang is a postgraduate student of College of Transportation and Vehicle Engineering, Shandong University of Technology, Zibo, Shandong, China (e-mail: 948541975@qq.com).

Shiwei Jin is a postgraduate student of College of Transportation and Vehicle Engineering, Shandong University of Technology, Zibo, Shandong, China (e-mail: 18502100129@stumail.sdut.edu.cn).

Kun Yang is a professor of College of Transportation and Vehicle Engineering, Shandong University of Technology, Zibo, Shandong, China (corresponding author, e-mail: yangkun@sdut.edu.cn).

Zhihao Li is an engineer of Kaima Automobile Manufacturing Co. LTD, Shouguang, Shandong, China (e-mail: lizhihao@kamaqc.com).

Compared with the EMS without the assistance of economy driving system, an adaptive strategy under MPC [22] can improve the fuel economy through HIL test. The calculation task of optimization-based strategy is enormous and the complex calculation is not acceptable for most practical applications. Therefore, the instantaneous optimal energy management strategy [23] such as MPC has developed rapidly and has been widely used for the benefits of real-time ability and good control effect.

Based on the analysis above, it is found that lots of scholars focus on the development of PHEV configuration and energy management strategy unilaterally. And only few scholars consider both fuel economy and real-time performance. Therefore, in this paper, the MPC strategy is developed with full consideration of vehicle economy and real-time application potential. In section II, dual motor coupled PHEV configuration is researched. In section III, the rule-based strategy and DP strategy are discussed. In section IV, three different vehicle speed prediction models for various time domain lengths are investigated. Besides, the model with the best speed prediction effect is selected and applied to the MPC strategy. Based on the DP algorithm and constraint functions, the MPC strategy is developed and analyzed to obtain the optimal control sequence. In section V, some conclusive remarks in the economy and real-time performance of PHEV under three strategies are given.

## II. CONFIGURATION AND MODELING OF DOUBLE MOTOR COUPLED PHEV

### A. Analysis of Vehicle Configuration and Dynamic Characteristics Introduction

The PHEV configuration is shown in Figure 1. The target PHEV is mainly composed of Motor-Generator 1(MG1), Motor-Generator 2 (MG2), engine and planetary gear mechanism. MG1 is connected with the sun gear of the planetary gear mechanism; MG2 is connected with the ring gear of the planetary gear through a fixed reduction gear  $i_1$ .

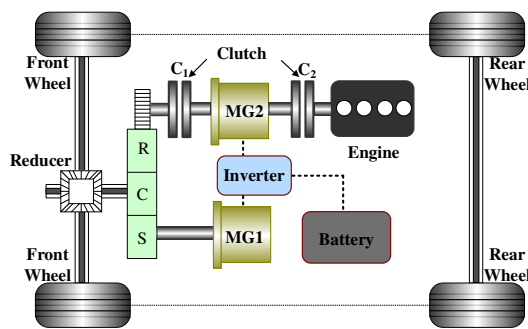


Fig. 1. The dual motor coupling configuration of PHEV

Based on the principle of electricity consumption priority, the PHEV can be operated under three pure electric operating modes when the battery energy is sufficient: MG1, MG2 and dual motor speed coupling operating mode. Similarly, the vehicle operating modes can be split into three conditions when the energy of battery pack is insufficient.

Case1: When vehicle speed is low, clutch C1 is disengaged and clutch C2 is engaged. The MG2 works as a generator and the engine drives MG2 to generate electricity. The target

vehicle works in the series operating mode and the generated MG2 power is supplied to MG1 to propel the vehicle.

Case2: When vehicle works at medium speed, the clutch C1 and C2 are both engaged. Only the engine drives the vehicle and the ring gear can transmit the engine power to the wheel.

Case3: When the vehicle works at high speed, the vehicle is driven by the engine and MG1 together.

To sum up, the vehicle operating mode can be adjusted automatically according to the battery power. The operation status of each component for the six operating modes is shown in Table 1.

TABLE I  
WORKING CONDITION DIAGRAM OF EACH COMPONENT  
(W= Work, C=Closed, L=Locked, D=Disengaged, E= Engaged)

Operating mode	MG1	MG2	Engine	Sun gear	Ring gear	C <sub>1</sub>	C <sub>2</sub>
MG1	W	C	C	W	L	D	D
MG2	C	W	C	L	W	E	D
Speed coupling	W	W	C	W	W	E	D
Series	W	W	W	W	L	D	E
Engine	C	W	W	L	W	E	E
Combined	W	W	W	W	W	E	E

### B. Dynamic Characteristics Analysis

#### 1) MG1 operating mode

The energy flow of the only MG1 operating mode is shown in Figure 2. MG1 drives the vehicle with the condition of sufficient battery pack energy, low velocity and small required power. The ring gear is locked. The clutch C1 and C2 are disengaged. The MG1 power can be transmitted to the wheel through the planetary gear. The dynamic relation is derived as shown in equation (1):

$$\begin{cases} \omega_c = \frac{\omega_{MG1}}{1+k} \\ T_c = (1+k)T_{MG1} \end{cases} \quad (1)$$

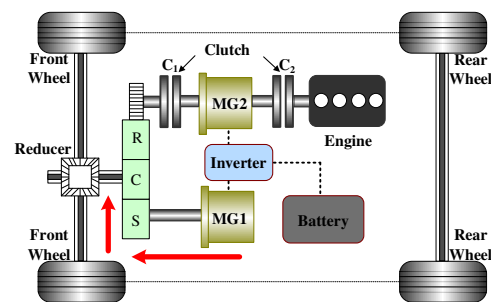


Fig. 2. Energy flow of MG1 operating mode

#### 2) MG2 operating mode

The energy flow of the only MG2 operating mode is shown in Figure 3. MG2 drives the vehicle with the condition of sufficient battery pack energy, medium velocity and small power demand. The sun gear is locked. The clutches C1, C2 are engaged and disengaged respectively. The MG2 power can be transmitted to the wheel through the planetary gear. The dynamic relation is derived as shown in equation (2):

$$\begin{cases} \omega_c = \frac{k \cdot \omega_{MG2}}{i_1 \cdot (1+k)} \\ T_c = \frac{i_1 \cdot (1+k)}{k} T_{MG2} \end{cases} \quad (2)$$

where  $\omega_c$  is the output speed of planetary carrier, rad/s;  $\omega_{MG1}$  and  $\omega_{MG2}$  are the MG1 and MG2 speed respectively, rad/s;  $k$  is the characteristic parameter of the planetary gear;  $T_c$  is planetary carrier torque, Nm;  $i_1$  is the fixed reduction gear ratio;  $T_{MG1}$  and  $T_{MG2}$  are the MG1 and MG2 torque respectively, Nm.

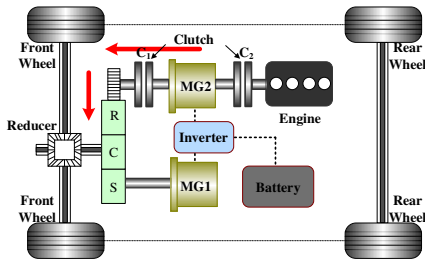


Fig. 3. Energy flow of MG2 operating mode

3) Dual motor speed coupling operating mode

The energy flow of this mode is shown in Figure 4. When the battery pack energy is sufficient and the velocity is high, the two motors are cooperated together to satisfy the speed requirement. Clutch C1 is engaged and clutch C2 is disengaged. The dynamic relation is derived as shown in equation (3):

$$\begin{cases} (1+k)\omega_c = \omega_{MG1} + \frac{k}{i_1} \cdot \omega_{MG2} \\ T_c = (1+k)T_{MG1} = \frac{i_1 \cdot (1+k)}{k} T_{MG2} \end{cases} \quad (3)$$

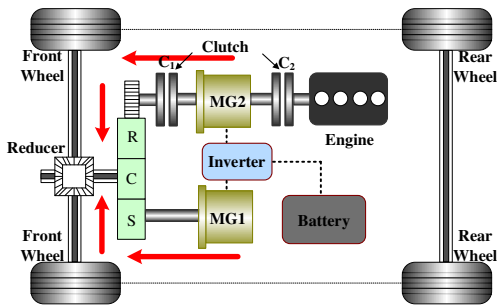


Fig. 4. Energy flow of dual motor speed coupling operating mode

4) Series operating mode

The energy flow of series operating mode is shown in Figure 5. The MG2 power is sent to the MG1 to propel the vehicle for the condition of insufficient battery energy, low vehicle speed and small power demand. At this time, the ring gear is locked, clutch C1 is disengaged and clutch C2 is engaged. The dynamic relation is derived as shown in equation (4):

$$\begin{cases} \omega_c = \frac{\omega_{MG1}}{1+k} \\ T_c = (1+k)T_{MG1} \\ T_{eng} = -T_{MG2} \\ \omega_{eng} = \omega_{MG2} \end{cases} \quad (4)$$

where,  $\omega_{eng}$  is the engine speed, rad/s;  $T_{eng}$  is the engine torque, Nm.

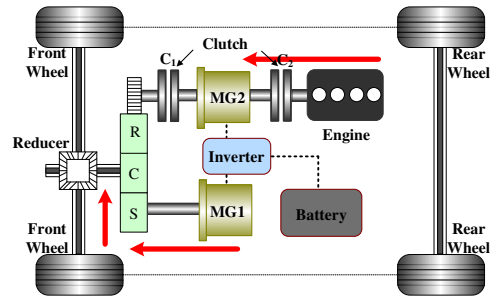


Fig. 5. Energy flow of series operating mode

5) Engine operating mode

The energy flow of engine operating mode is shown in Figure 6. The engine drives the vehicle alone with the condition of low battery pack energy and medium/high velocity. At this time, the sun gear is locked, and the clutches C1, C2 are engaged. The dynamic relation is derived as shown in equation (5):

$$\begin{cases} \omega_c = \frac{k \cdot \omega_{eng}}{i_1 \cdot (1+k)} \\ T_c = \frac{i_1 \cdot (1+k)}{k} (T_{eng} + T_{MG2}) \\ T_{MG2} = -(T_{eng} - T_{req}) \\ \omega_{eng} = \omega_{MG2} \end{cases} \quad (5)$$

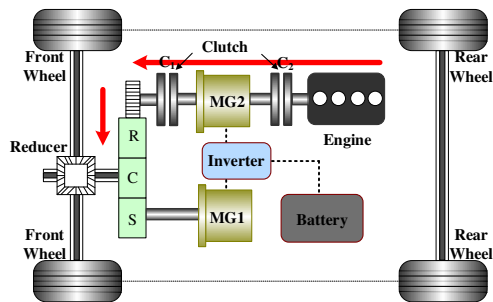


Fig. 6. Energy flow of engine operating mode

6) Combined operating mode

The energy flow of combined operating mode (engine, MG1 and MG2) is expressed in Figure 7. When the battery pack energy is insufficient and the vehicle works at a high velocity, the engine, MG1 and MG2 drive the vehicle together. At this time, the MG2 can be used as either a motor or a generator to adjust the engine optimal operating. The clutch C1 and C2 are engaged. The dynamic relation is derived as shown in equation (6):

$$\begin{cases} (1+k)\omega_c = \omega_{MG1} + \frac{k}{i_1} \cdot \omega_{eng} \\ T_c = (1+k)T_{MG1} = \frac{i_1 \cdot (1+k)}{k} (T_{eng} + T_{MG2}) \\ \omega_{eng} = \omega_{MG2} \end{cases} \quad (6)$$

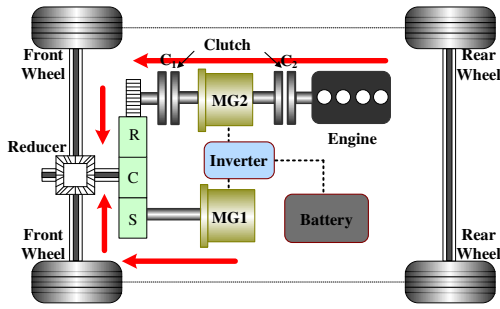


Fig. 7. Energy flow of combination operating mode

C. Core Components and Vehicle Model

The parameter matching of vehicle components are performed based on the vehicle performance index, as shown in Table 2. Detailed parameter matching process will not be discussed in this paper.

The full PHEV model is established by MATLAB/Simulink/Stateflow with the combination of vehicle component such as motor, engine, battery, clutch, planetary gear etc. The full vehicle model is shown in Figure 8.

TABLE II  
VEHICLE PARAMETERS

Parameters	Value	Unit
Full mass	1750	kg
Frontal area	2.35	m <sup>2</sup>
Maximum engine power	75	kW
maximum engine speed	6500	rpm
Maximum engine torque	135	Nm
MG1 rated/peak power	15/30	kW
MG1 rated/peak torque	70/145	Nm
MG1 rated/peak speed	2000/6200	rpm
MG2 rated/peak power	30/60	kW
MG2 rated/peak speed	3000/7500	rpm
MG2 rated/peak torque	95/190	Nm
Characteristics of planetary gear k (R/S)	2.5	-
Final ratio $i_0$	3.5	-
Reduction ratio $i_1$	1.6	-
Battery capacity	40	A·h
Battery rated voltage	360	V

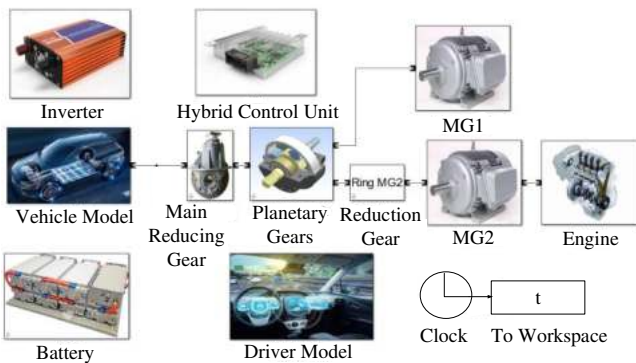


Fig. 8. Full vehicle model of the target PHEV

III. RULE-BASED AND DYNAMIC PROGRAMMING BASED EMS FOR PHEV

A. Rule-based Energy Management Strategy

1) Principle of rule-based energy management strategy

Since the cost of electricity is relatively cheap than fuel, the PHEV will work in the electric operating mode until the battery State of Charge (SOC) drops to the bottom line. Based on the change trajectory of the battery SOC, the PHEV operating modes can be divided into Charge Depleting (CD) mode and Charge Sustaining (CS) mode. The schematic diagram of regular CD-CS strategy is expressed in Figure 9.

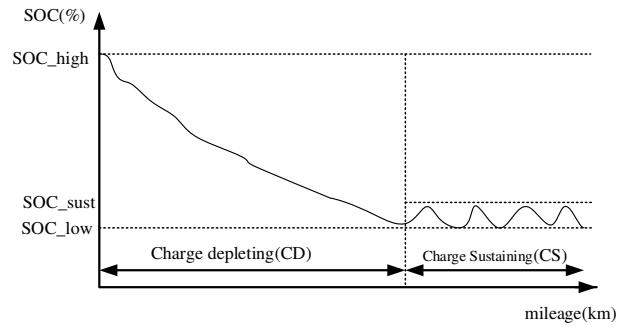


Fig. 9. Regular CD-CS control strategy

Since the battery SOC is high in CD mode and the electric driving is cost-effective than that of fuel drive, MG1 and MG2 drive the vehicle together. In this stage, the electricity is the only energy source and the battery SOC is decreasing in this stage.

In the CS mode, the engine and two motors drive the vehicle coordinately. Besides, the engine is the main energy source. The engine can provide the required vehicle power and provide additional power to keep battery SOC in a reasonable value.

2) Formulation of rule-based energy management strategy

The multi-power sources of PHEV bring various operating modes and relatively complicated EMS. Rule-based strategy has the benefits of simple formulation and high application, so the rule-based strategy is selected as the benchmark strategy in this paper. In Figure 10, the rule-based strategy is explained.

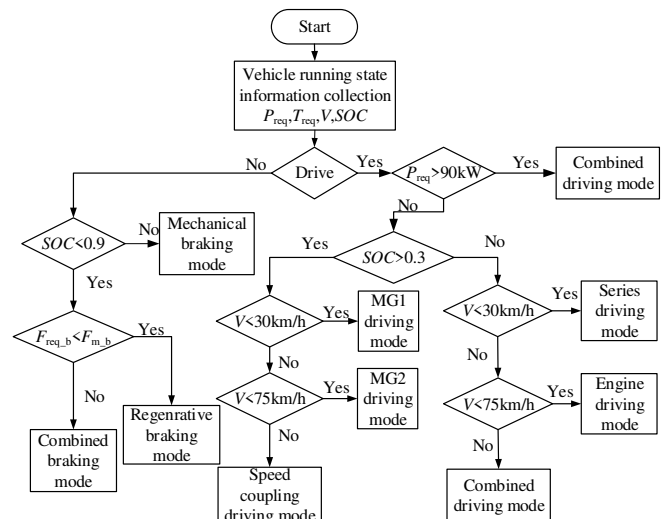


Fig. 10. Mode switching algorithm based on rule-based strategy

It is seen from Figure 10 that different operating modes can be selected depending on relevant vehicle parameters.

### B. Dynamic Programming Based Energy Management Strategy

#### 1) Principle of dynamic programming algorithm

Dynamic programming is the most common method to solve multi-stage decision optimization problem. In this problem, several interacting stages constitute the multi-stage decision. Each stage includes a decision problem. At the same time, the decision of each stage and its results will affect next stage. Then the decision of each stage constitutes a decision sequence [24]. The schematic diagram of multi-stage decision making problem is shown in Figure 11.



Fig. 11. Schematic diagram of multi-stage decision making problem

For a given multi-stage decision system, the cost function of each stage and the optimal control sequence are combined to achieve global optimization by reverse solution.

#### 2) Problem construction of dynamic programming algorithm

In this paper, battery SOC is chosen as the system state variable and there is a certain dynamic relationship in the planetary gear dynamic coupling mechanisms.

At the same time, the output torque of planet carrier has proportional relationship with the input torque of ring gear and sun gear. Therefore, the engine torque  $T_{eng}$  and MG2 speed  $\omega_{MG2}$  are selected as the system control variables. The selected state variables and control variables are described in equation (7).

$$\begin{cases} x(k) = SOC(k) \\ u(k) = [T_{eng}(k), \omega_{MG2}(k)] \end{cases} \quad (7)$$

The system state equation (8) is obtained.

$$SOC(k+1) = SOC(k) - \frac{U_{oc}(k) - \sqrt{U_{oc}^2(k) - 4 \cdot R_{int}(SOC(k)) \cdot P_{bat}(k)}}{2 \cdot R_{int}(SOC(k)) \cdot Q_{bat}} \quad (8)$$

In equation (8),  $P_{bat}(k)$  can be derived by equation (9).

$$P_{bat}(k) = \frac{P_{MG1}(k)}{\eta} + \frac{P_{MG2}(k)}{\eta} \quad (9)$$

where  $P_{MG1}$  and  $P_{MG2}$  are the power of MG1 and MG2 respectively, kW.

Firstly, the optimization objective function in the time domain of k-time prediction is established as shown in equation (10).

$$J_k = \sum_{t=k}^{k+p} L(x(t), u(t)) = \sum_{t=k}^{k+p} (\alpha_f \cdot fuel(k) + \alpha_e P_{bat}(k) / 3600 + \alpha (SOC(k) - SOC_f)^2) \quad (10)$$

where  $L$  is the instantaneous optimization function, and  $L$  changes with the change of prediction time domain;  $\alpha_f$  is the

oil price, 7 RMB/L;  $fuel(k)$  is the fuel consumption at a certain stage;  $\alpha_e$  is the electricity price, 0.6 RMB/kWh;  $SOC_f$  is the SOC value at the end time;  $\alpha (SOC(k) - SOC_f)^2$  is the penalty function of the model and the penalty coefficient  $\alpha$  is a large value to avoid the SOC drops too fast.

In order to make the solution reasonable and reduce the calculation time, the following constraints should be added, as shown in equation (11).

$$\begin{cases} \omega_{eng\_min}(k) \leq \omega_{eng}(k) \leq \omega_{eng\_max}(k) \\ \omega_{MG1\_min}(k) \leq \omega_{MG1}(k) \leq \omega_{MG1\_max}(k) \\ \omega_{MG2\_min}(k) \leq \omega_{MG2}(k) \leq \omega_{MG2\_max}(k) \\ T_{eng\_min}(\omega_e(k)) \leq T_{eng}(k) \leq T_{eng\_max}(\omega_e(k)) \\ T_{MG1\_min}(\omega_{MG1}(k)) \leq T_{MG1}(k) \leq T_{MG1\_max}(\omega_{MG1}(k)) \\ T_{MG2\_min}(\omega_{MG2}(k)) \leq T_{MG2}(k) \leq T_{MG2\_max}(\omega_{MG2}(k)) \\ SOC_{min} \leq SOC(k) \leq SOC_{max}(k) \end{cases} \quad (11)$$

where the subscript eng represents the engine and the subscripts min and max represent the upper and lower limits of the value respectively.

## IV. MODEL PREDICTIVE CONTROL BASED ENERGY MANAGEMENT STRATEGY FOR PHEV

### A. Introduction of Model Predictive Control

The DP based energy management strategy has excellent performance in improving fuel economy. However, due to the complex calculation of global optimization, the DP algorithm is difficult to be applied in real vehicle. Therefore, model predictive control strategy is proposed on the basis of DP methodology with the consideration of fuel economy and real-time application. MPC control schematic diagram is shown in Figure 12.

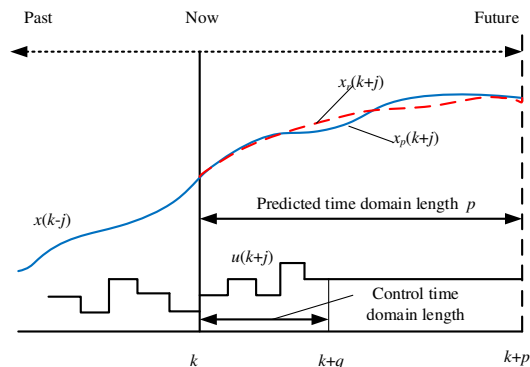


Fig. 12. MPC control schematic diagram

The two most important steps of model predictive control are rolling optimization and prediction model selection. Rolling optimization is not a global optimization. It needs to determine the optimization goal in the current time domain and gradually complete the overall optimization. Rolling optimization is a unique advantage of MPC, which is also the biggest difference from DP algorithm.

The prediction model can predict the future state of the system. In this paper, three different prediction models are discussed to obtain the best speed prediction time domain. Specific solutions are covered in section IV.B.

**B. Evaluation Standard of Vehicle Future State Prediction**

The prediction of the vehicle future state is realized based on historical information and current information. According to the prediction model, the vehicle running state in the finite prediction time domain is predicted. The precision of predicted vehicle state also influences the accuracy of the energy management strategy. So, the prediction method should be reasonably selected.

In order to verify the accuracy of speed prediction, root mean square error (RMSE) is used as the evaluation index, as shown in equation (12)-(13).

$$R(k) = \sqrt{\sum_{i=1}^p (v_p(k+i) - v_r(k+i))^2 / p} \tag{12}$$

$$Re = \sqrt{\sum_{k=1}^S R^2(k) / S} \tag{13}$$

where  $R(k)$  is the root mean square error in the prediction time domain;  $Re$  is the total root mean square error;  $v_p(k+i)$  is the predicted speed at that time,  $v_r(k+i)$  is the actual speed. The value of  $Re$  has an inverse relationship with the prediction result.

Therefore, the index prediction, Markov prediction and neural network prediction are applied to predict the vehicle operation status information.

In this paper, four different working conditions are selected as the sample condition. The working conditions are shown in Figure 13.

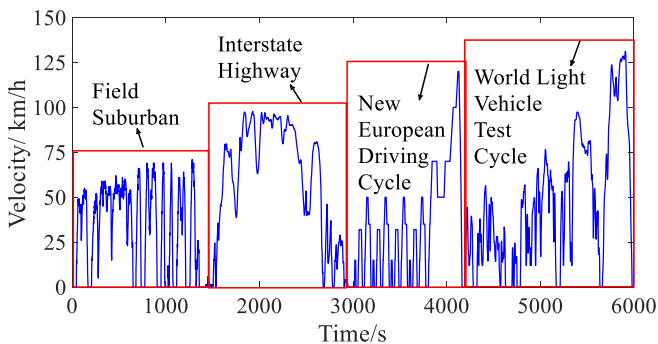


Fig. 13. Sample condition

**1) Prediction Based On Index Model**

Index function, as a common prediction model, is used to predict the future development trend. In the aspect of vehicle running state prediction, the index prediction model can predict the future vehicle acceleration and further obtain the predicted speed.

The specific implementation is as follows: according to the acceleration  $a(k)$ , the acceleration sequence within  $k \sim k+p$  can be obtained from equation (14). Then the current acceleration, speed and the future speed series in  $k \sim k+p$  can be further obtained from equation (15).

$$a(k+i) = a(k) * \exp\left(-\frac{i}{\tau}\right), i=1,2,\dots,p \tag{14}$$

$$v(k+i) = v(k) + \int_k^{k+i} a(x)dx \tag{15}$$

where  $a(k+i)$  is the acceleration at the time of  $k+i$ ;  $\tau$  is the recession factor of the function. Under different time-domain length, the prediction effect is different due to the different values of  $\tau$ .

For different prediction time-domain length, the value of  $\tau$

is also different when reaches the best predication accuracy. The optimal  $\tau$  value is used for the prediction simulation analysis in different forecast time-domains. The simulation effects of different prediction time are shown in Figure 14.

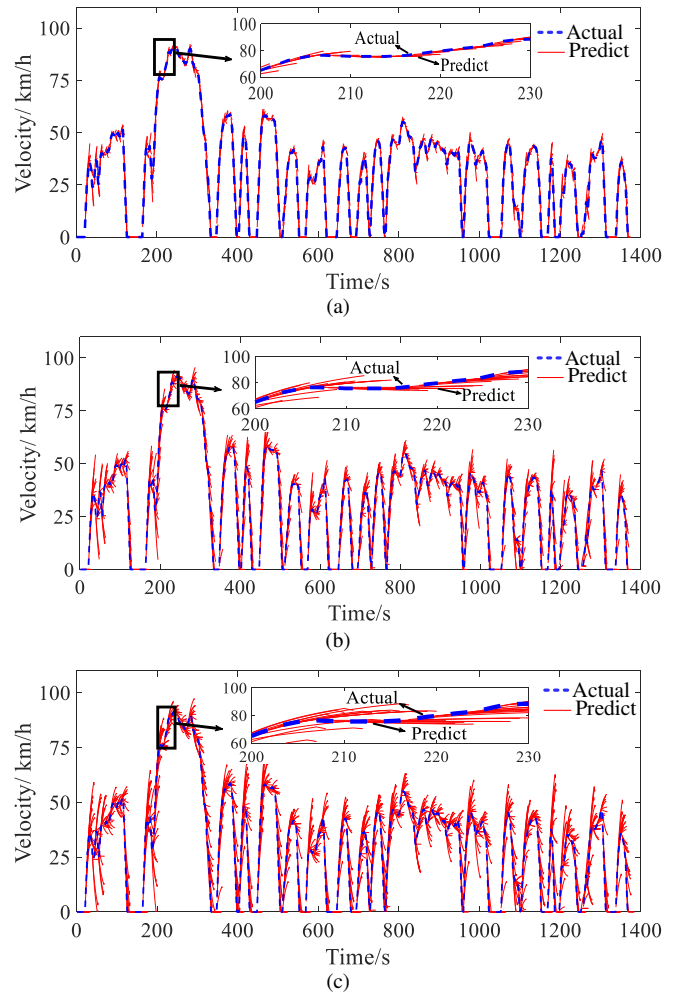


Fig. 14. Forecast effect of index model prediction. (a)  $p=5s$ . (b)  $p=10s$ . (c)  $p=15s$ .

**2) Prediction Based On Markov Model**

Since the vehicle driving is affected by several external factors, the change of vehicle speed (acceleration) is a random process. Markov model is a sequence of random variables. The system state at a certain time in the future only relies on the present time state. Therefore, the system state at any time in the future can be inferred from the current system state instead of the historical state.

In Markov model, the sampling step is set as 1s, and the speed and acceleration are discretized at appropriate intervals. The nearest neighbor method can be used to obtain the speed and acceleration state values in all state spaces, as shown in equation (16).

$$\begin{cases} v \in \{v^1, v^2, \dots, v^l\} \\ a \in \{a^1, a^2, \dots, a^r\} \end{cases} \tag{16}$$

The sum of the acceleration transfer times can be obtained from equation (17). Then the maximum likelihood estimation method can be applied to calculate the acceleration probability corresponding to discrete vehicle speed, as shown in equation (18).

$$m_{n,i} = \sum_{j=1}^r m_{n,i,j} \tag{17}$$

$$P_{n,i,j} = \frac{m_{n,i,j}}{m_{n,i}} \tag{18}$$

At each speed, one-step state transition probability matrix P can be obtained. Multiple transition probability matrices are constructed into one-step Markov model. The one-step transition probability matrix of acceleration at 35km/h is shown in Figure 15.

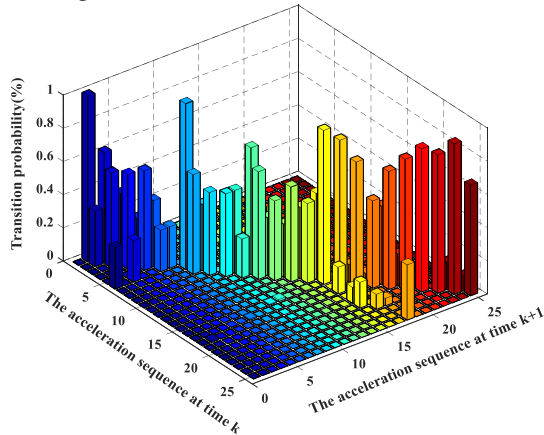


Fig. 15. One step transition probability matrix model

The above process is repeated until vehicle speed and acceleration in the whole prediction time domain are obtained. The prediction effect in each prediction time domain is shown in Figure 16.

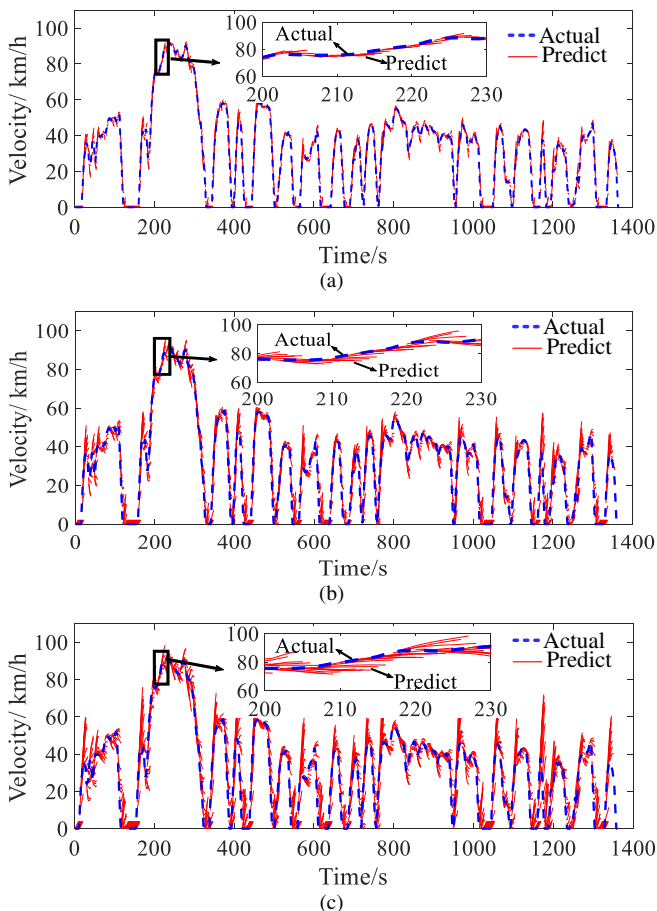


Fig. 16. Forecast effect of Markov model. (a) p =5s. (b) p =10s. (c) p =15s.

3) Prediction Based On RBF Neural Network Model

The RBF neural network is generally displayed as Gauss function. Therefore, the activation function of RBF neural network can be expressed as equation (19).

$$R(x_p - c_i) = \exp\left(-\frac{1}{2\sigma^2} \|x_p - c_i\|^2\right) \tag{19}$$

where  $\|x_p - c_i\|$  is the European norm;  $c_i$  is the center of the Gaussian function.

Therefore, the output of RBF neural network can be expressed as equation (20).

$$y_i = \sum_{j=1}^h \omega_{ij} \exp\left(-\frac{1}{2\sigma^2} \|x_p - c_j\|^2\right) \quad j = 1, 2, \dots, n \tag{20}$$

where,  $x_p$  is the input sample;  $c_i$  is the center of the hidden layer node;  $\omega_{ij}$  is the connection weight between the hidden layer and the output layer;  $y_i$  is the actual output of the input sample.

The historical vehicle speed and current vehicle speed information are the input variables of the neural network. The predicted speed in the prediction time domain is the output. The number of neurons in the neural network is 30. The mapping relationship is derived as shown in equation (21).

$$[v_{k+1}, v_{k+2}, \dots, v_{k+p}] = f_{RBF}(v_{k-h+1}, \dots, v_k) \tag{21}$$

where  $v$  is the driving speed;  $h$  is the number of input historical speeds;  $f_{RBF}$  is the mapping relationship between input and output of RBF neural network;  $p$  is the prediction length in time domain.

The RBF prediction model is developed using MATLAB to obtain the single-step prediction result in Figure 17 (a). As seen in Figure 17 (b), most of the single-step prediction errors are less than 0.1km/h, and the errors of other individual points are also within 1km/h. The developed RBF model has good prediction result and high accuracy, so it can be further studied.

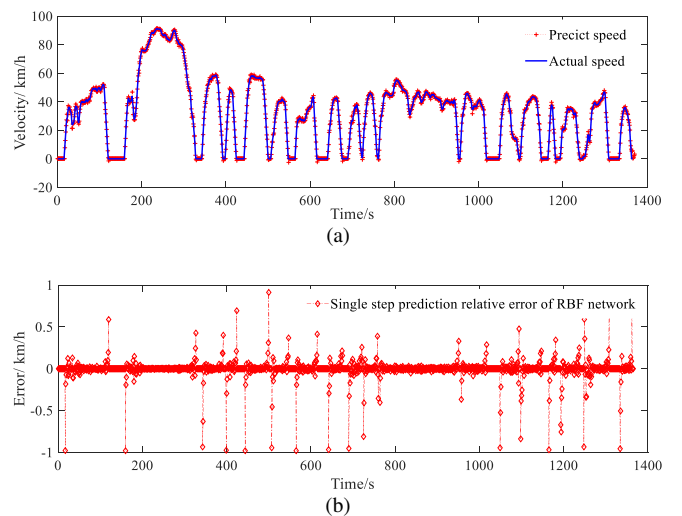


Fig. 17. RBF prediction model single step prediction diagram. (a) single-step prediction result. (b) single-step prediction relative error.

The prediction results of different prediction time domains of RBF neural network model are shown in Figure 18.

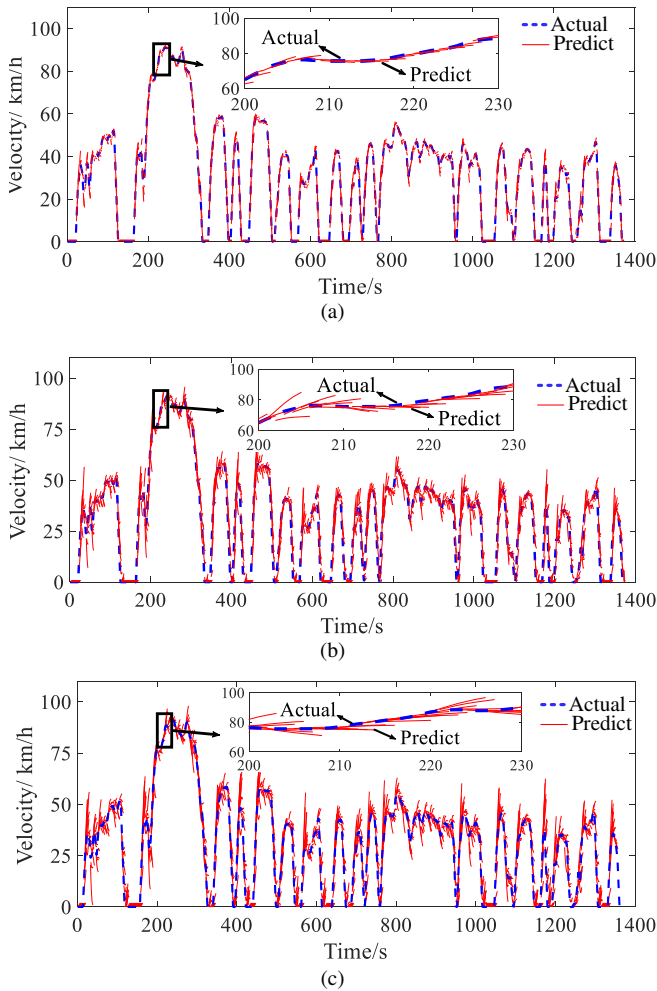


Fig. 18. Forecast effect chart of RBF model. (a)  $p=5s$ . (b)  $p=10s$ . (c)  $p=15s$ .

4) Prediction Model Selection

The prediction results of different prediction models under different prediction time domain lengths are expressed in Table 3. The root mean square error of different prediction models under the same prediction time domain is shown in Figure 19.

TABLE III

PREDICTION EFFECT UNDER DIFFERENT PREDICTION MODELS

Predict time domain $p$	RMSE under Index model prediction	RMSE under Markov model prediction	RMSE under RBF model prediction
5s	2.7521	1.9136	1.7913
10s	5.4615	4.6554	4.3538
15s	10.3855	8.9699	8.0255

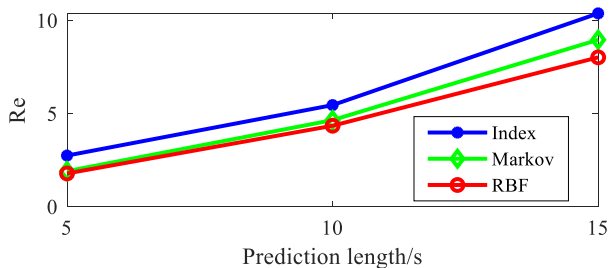


Fig. 19. Comparison chart of prediction effort for different models

It is seen from Figure 19 that the prediction accuracy of

three prediction methods has inverse relationship with the prediction time domain. The RBF neural network prediction model is the most accurate prediction model in the same prediction time domain. Therefore, the RBF neural network model is chosen in the subsequent model prediction algorithm. Considering comprehensively, 10s is selected as the prediction time domain length.

C. Solution of Model Predictive Control Problem

Based on the battery SOC reference trajectory and RBF neural network prediction model, the rolling optimization of MPC can be realized using DP algorithm framework and constraint equation (8) - (11). The solution process is shown in Figure 20.

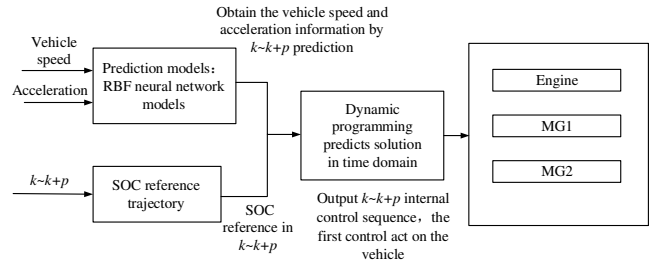


Fig. 20. MPC solution flow chart

V. ANALYSIS OF SIMULATION RESULTS

A. Analysis of Fuel Economy

In this paper, six UDSS driving conditions are selected as the test condition. Initial and termination battery SOC are set as 0.7 and 0.3 respectively. The prediction step is 10s under RBF neural network. Based on the above conditions, rule-based (CD-CS) strategy, DP strategy and MPC strategy are verified. The simulation results of battery SOC in the above strategies are shown in Figure 21.

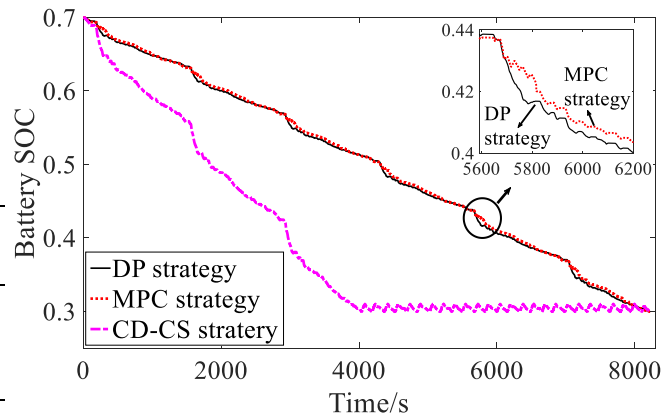


Fig. 21. Comparison of battery SOC for three algorithms

It is seen in Figure 21, battery SOC in the rule-based strategy decreases rapidly and then fluctuates around 0.3. Since the fuel and electricity are reasonably distributed by the global optimization of the DP algorithm, the battery SOC of the DP algorithm decreases slowly. Similarly, with the limitation of reference trajectory and constraints, the battery SOC of the MPC algorithm decreases slowly.

The engine working point can be analyzed for three energy management strategies, as shown in Figure 22.

As seen in Figure 22, since the rule-based strategy is not

flexible, the operation points of engine are more scattered in low efficiency area and the fuel economy is poor. The engine working points of DP algorithm are more scattered around the high-efficiency area of optimal working curve. The engine working points of MPC algorithm are also dispersed in high-efficiency area. However, the MPC algorithm only predicts the local optimal in time domain. The global energy management strategy is approximating optimal. The MPC cannot predict more driving information in the future. Therefore, some engine working points are dispersed in the low efficiency range. Nevertheless, the whole vehicle economy is greatly improved in comparison with the rule-based strategy.

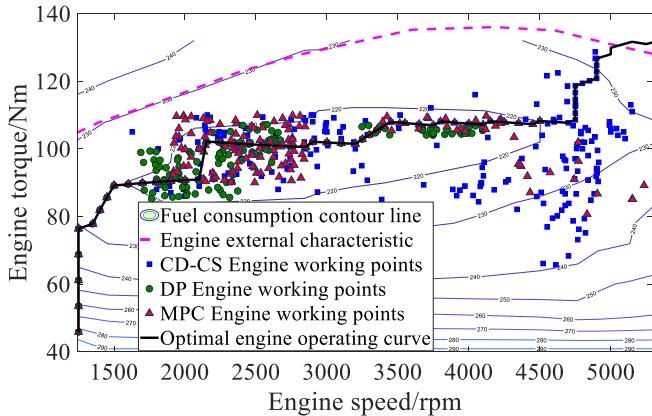


Fig. 22. Comparison of engine operating points for three algorithms

As shown in Figure 23, the fuel consumption results for three energy management strategies are obtained. Since the electric power of rule-based (CD-CS) strategy is sufficient at  $t=0-4000s$ , the vehicle is driving under CD mode with the fuel consumption of zero. When the battery SOC drops to the bottom value, the vehicle is driving under CS mode with sharply rising fuel consumption. For the DP strategy and MPC strategy, the engine and motor are reasonable controlled by optimization algorithm. Therefore, the fuel consumption curves rise slowly with similar changing trend. As for the fuel consumption of the three strategies, the fuel consumption of DP strategy and MPC strategy is smaller than rule-based strategy.

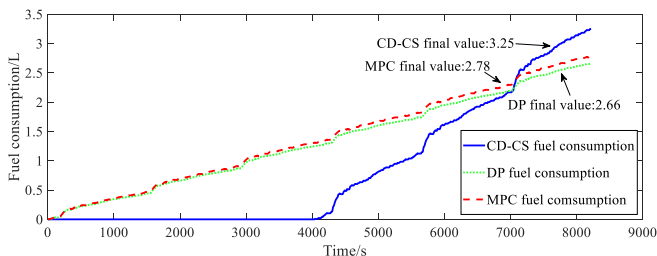


Fig. 23. Comparison of fuel consumption for three algorithms

Then, the cost for different algorithms are calculated with the combination of the fuel consumption and electricity (The electricity price is 0.6 RMB/kWh, and the gasoline price is 7 RMB/L), as shown in Table 4.

It is seen from Table 4 that the MPC strategy has similar total cost with DP strategy, while the rule-based strategy has higher total cost compared with DP and MPC strategies. To further confirm the validity of MPC strategy, the fuel cost and

total cost of MPC strategy are further compared and analyzed in Table 5. The fuel cost and total cost of MPC strategy is significantly reduced by 14.5% and 12.6% respectively in contrast to rule-based strategy, which proves the validity of the proposed MPC strategy.

TABLE IV  
COST COMPARISON OF DIFFERENT OPTIMIZATION ALGORITHM

Working condition	Proposed strategy	Fuel cost/L	Electricity cost/kWh	Total cost /RMB
Working condition of UDDS	Rule strategy	3.25	5.7672	26.21
	DP strategy	2.66	5.7586	22.08
	MPC strategy	2.78	5.7514	22.91

TABLE V  
COMPARISON AND ANALYSIS OF MPC AND RULE STRATEGIES

-	Rule strategy	MPC strategy	Improvement
Fuel cost/L	3.25	2.78	14.5%
Total cost/RMB	26.21	22.91	12.6%

B. Real Time Performance Analysis

In win7 system, CPU i5-4460, 3.2GHz, memory 16GB desktop computer, the RBF prediction model is verified. The results are expressed in Table 6.

TABLE VI  
REQUIRED OPERATING TIME AT DIFFERENT PREDICTED LENGTHS

-	Prediction length 5s	Prediction length 10s	Prediction length 15s
1 UDDS working condition prediction time	1.75s	1.98s	2.89s
Single step prediction time	1.27ms	1.45ms	2.11ms

As shown in Table 6, the prediction time has the linear relation with the prediction time domain. Under the whole UDDS condition, the prediction time increases from 1.75s to 2.89s, and the single step prediction time increases from 1.27ms to 2.11ms. The single step prediction time is relatively short, so the single step prediction has certain real-time application potential. Considering the accuracy and rapidity of the prediction in time domain, it is reasonable to select 10s as the prediction step.

TABLE VII  
CALCULATION TIME OF MPC

-	Consumption time/s
6 UDDS working condition prediction time	2213
Conversion to single step calculation time	0.269

As shown in Table 7, the total calculation time is 2213s under 6 UDDS conditions and the single step calculation time is 0.269s. With the reduction of the prediction time, the calculation time is reduced. Meanwhile, the cost of the whole vehicle is also reduced. Therefore, the 10s is selected as the prediction step for better economy improvement and certain

real-time application potential.

## VI. CONCLUSION

In this paper, model predictive control based energy management strategy is developed for dual motor coupled PHEV configuration. The PHEV powertrain model is constructed using MATLAB/Simulink/Stateflow. Then, the rule-based strategy and DP strategy are established. The DP strategy can improve operation efficiency of power components under different working conditions while the real-time performance is poor. The rule-based strategy has opposite characteristics with the DP strategy. Considering the vehicle economy and real-time application potential, MPC strategy is developed. Under RBF neural network prediction model, DP algorithm framework and constraint functions, the economy and real-time performance of MPC strategy are verified.

The results show that: MPC strategy can obtain similar fuel consumption compared DP strategy, while the calculation time of MPC strategy has real-time application potential with only 0.269s per single step calculation time. The fuel cost and total cost of MPC strategy is significantly reduced by 14.5% and 12.6% respectively in comparison with the rule-based strategy. Therefore, MPC strategy not only improves fuel economy, but also has application potential in real time.

## REFERENCES

- [1] N. Soares, A. G. Martins, A. L. Carvalho, C. Caldeira, C. Du, E. Castanheira, E. Rodrigues, G. Olivera, G. I. Pereira, J. Bastos, J. P. Ferreira, L. A. Ribeiro, N. C. Figueiredo, N. Sahovic, P. Miguel, R. Garcia, "The challenging paradigm of interrelated energy systems towards a more sustainable future," *Renewable and Sustainable Energy Reviews*, vol. 95, pp171-193, 2018.
- [2] Wang Y, Jiao X, Sun Z, Li P, "Energy management strategy in consideration of battery health for PHEV via stochastic control and particle swarm optimization algorithm," *Energies*, vol.10, no.11, 1894, 2017.
- [3] C. M. Martinez, Hu X, Cao D, E. Velenis, Gao B. M. Wellers, "Energy management in plug-in hybrid electric vehicles: Recent progress and a connected vehicles perspective," *IEEE Transactions on Vehicular Technology*, vol. 66, no.11, pp4534-4549, 2016.
- [4] J. M. Miller, "Hybrid electric vehicle propulsion system architectures of the e-CVT type," *IEEE Transactions on Power Electronics*, vol.21, no 3, pp756-767, 2006.
- [5] Zhuang W, Zhang X, Zhao D, Peng H, Wang L, "Optimal design of three-planetary gear power-split hybrid powertrains," *International Journal of Automotive Technology*, vol.17, no.2, pp299-309, 2016.
- [6] Pei H, Hu X, Yang Y, Tang X, Hou C, Cao D, "Configuration optimization for improving fuel efficiency of power split hybrid powertrains with a single planetary gear," *Applied Energy*, vol. 214, pp103-116, 2018.
- [7] C. T. Chung, Y. H. Hung, "Energy improvement and performance evaluation of a novel full hybrid electric motorcycle with power split e-CVT," *Energy conversion and management*, vol.86, pp216-225, 2014.
- [8] Ju F, Zhuang W, Wang L, "A Novel Four-Wheel-Drive Hybrid Electric Sport Utility Vehicle with Double Planetary Gears," *IFAC PAPERSONLINE*, vol. 51, no.31, pp81-86, 2018.
- [9] Zhang F, Hu X, R. Langari, Cao D, "Energy management strategies of connected HEVs and PHEVs: Recent progress and outlook," *Progress in Energy and Combustion Science*, vol. 73, pp235-256, 2019.
- [10] M. G. Carignano, R. Costa-Castelló, V. Roda, N. M. Nigro, S. Junco, D. Feroldi, "Energy management strategy for fuel cell-supercapacitor hybrid vehicles based on prediction of energy demand," *Journal of power sources*, vol.360, pp419-433, 2017.
- [11] Liu J, Peng H, "Modeling and Control of a Power-Split Hybrid Vehicle," *IEEE Transactions on Control Systems Technology*, vol. 16, no.6, pp1242-1251, 2008.
- [12] Yu Z, M. Dawei, Z. Meilan, L. Dengke, "Management strategy based on genetic algorithm optimization for PHEV," *International Journal of Control and Automation*, vol. 7, no.11, pp399-408, 2014.
- [13] Li P, Li Y, Wang Y, Jiao X, "An intelligent logic rule-based energy management strategy for power-split plug-in hybrid electric vehicle," 2018 37th Chinese Control Conference (CCC), Wuhan, July. 25-27, pp7668-7672, 2018.
- [14] Wang Y, Jiao X, "Multi-objective energy management for PHEV using Pontryagin's minimum principle and particle swarm optimization online," *Science China (Information Sciences)*, vol. 64 no.1, pp.263-265, 2021.
- [15] Chih-Keng Chen, Tri-Vien Vu, Chih-Wei Hung, "Control strategy development and optimization for a series hydraulic hybrid vehicle," *Engineering Letters*, vol. 21 no. 2, pp. 101-107, 2013.
- [16] V. Larsson, L. Johannesson, B. Egardt, "Analytic solutions to the dynamic programming subproblem in hybrid vehicle energy management," *IEEE Transactions on Vehicular Technology*, vol. 64, no.4, pp1458-1467, 2015.
- [17] H. Nafisi, S. M. M. Agah, H. A. Abyaneh, M. Abedi, "Two-stage optimization method for energy loss minimization in microgrid based on smart power management scheme of PHEVs," *IEEE Transactions on Smart Grid*, vol. 7, no.3, pp1268-1276, 2016.
- [18] Meo, "Nonlinear convex optimization of the energy management for hybrid electric vehicles," *Engineering Letters*, vol. 22 no. 4, pp. 170-182, 2014.
- [19] Fan L, Zhang Y, Dou H, Zou R, "Design of an integrated energy management strategy for a plug-in hybrid electric bus," *Journal of Power Sources*, vol. 448, 227391, 2020.
- [20] C. Silva, M. Ross, T. Farias, "Evaluation of energy consumption, emissions and cost of plug-in hybrid vehicles," *Energy Conversion and Management*, vol. 50, no. 7, pp1635-1643, 2009.
- [21] M. Vajedi, A. Taghavipour, N. L. Azad, "Traction-motor power ratio and speed trajectory optimization for power split PHEVs using route information," *ASME 2012 International Mechanical Engineer Congress and Exposition*, vol. 45271, pp301-308, 2012.
- [22] Guo J Q, He H W, Peng J K, Z. Nana, "A novel MPC-based adaptive energy management strategy in plug-in hybrid electric vehicles," *Energy*, vol. 175, pp378-392, 2019.
- [23] Zhang Y, Chu L, Fu Z, Xu N, Guo C, Zhang X, Wang P, "Optimal energy management strategy for parallel plug-in hybrid electric vehicle based on driving behavior analysis and real time traffic information prediction," *Mechatronics*, vol. 46, pp177-192, 2017.
- [24] Li L, Yang C, Zhang Y, Zhang L, Song J, "Correctional DP-based energy management strategy of plug-in hybrid electric bus for city-bus route," *IEEE Transactions on Vehicular Technology*, vol.64, no. 7, pp 2792-2803, 2014.